International Journal of Thin Films Science and Technology

http://dx.doi.org/10.18576/ijtfst/150109

Removal of Fe(II) from Aqueous Solutions by *Corchorus olitorius* Stem Biochar as a Cost-Effective Biosorbent

Ahmed A.I. Abd-Ellatif [1,2], Mohamed N. Rashed[2], Mohamed A.M. Raslan[2,3], Salah G.A. Ali[4] and Gomaa A.M. Ali[5,]*

[1] Sohag Drinking Water, Sanitation Company, 82515, Sohag, Egypt
[2] Department of Chemistry, Faculty of Science, Aswan University, 81528, Aswan, Egypt
[3] Faculty of Technological Industry and Energy, Thebes Technological University, 85863, Thebes, Luxor, Egypt
[4] Department of Botany and Microbiology, Faculty of Science, Al-Azhar University,71524, Assiut, Egypt
[5] Sharjah Marine Science Research Centre, College of Marine Science and Aquatic Biology, University of Khorfakkan, Khor Fakkan, 18119, Sharjah, United Arab Emirates

Received: 2 Nov. 2025, Revised: 12 Dec. 2025, Accepted: 27 Dec. 2025
Published online: 1 Jan. 2026

Abstract: This study used *Corchorus olitorius* stem biochar (COSB) as a biosorbent with a high specific surface area (88.2 m^2/g) to remove Fe(II) at a reasonable cost. To identify the most effective Fe(II) removal method, a variety of removal parameters were investigated, including the pH, adsorbent dose, contact period, and initial Fe(II) concentration. The fitted equilibrium data were precisely characterized and analyzed using the Freundlich, Temkin, Langmuir, and Dubinin-Radushkevich models. Langmuir isotherm model R^2 (0.9907), which has a maximum saturated monolayer sorption capacity of 83.33 mg/g, was found to well represent the developed method. The adsorption process followed pseudo-second-order kinetics, as demonstrated by the high value of R^2 (0.9977) and the good agreement between the experimental value of q_e (43.5 mg/g) and the calculated value of q_e (47.17 mg/g). The adsorption process was conducted at different temperatures to evaluate the influence of temperature on the thermodynamic parameters. The spontaneity of the process is demonstrated by consistently negative values of ΔG^o over a broad temperature range. The adsorption process was observed to be endothermic ($\Delta H^o = +18.76$ kJ/mol). The positive value of ΔS^o suggests an increase in randomness at the solid/solution interface of Fe(II) with the adsorbent. The experimental results showed that COSB had a remarkable effect on Fe(II) removal from aqueous solutions.

Keywords: Adsorption, *Corchorus olitorius* Stem Biochar (COSB), Water Treatment, Environment.

1 Introduction

In many nations with limited surface water, groundwater serves as the primary source of drinking and agricultural water [1, 2]. For instance, groundwater is the only source of water in some desert regions, such as Saudi Arabia and the Middle East. Additionally, almost 70% of the water used in many European nations (Austria, Belgium, Denmark, Hungary, Romania, and Switzerland) is derived from groundwater. Furthermore, practically all the water in places such as Rome and Budapest comes from groundwater [3]. Because the water supply is frequently near customers, groundwater is also preferable [4]. Groundwater is the primary source of drinking water in rural and nomadic regions of Egypt. Groundwater is usually considered the best source of drinkable water if adequately shielded from contamination. Egypt's demand for potable water is increasing as its population grows.

The most common problem limiting groundwater use in Egypt is the high concentration of iron and manganese. Iron (Fe) is found in the earth's crust at an average of 6.22%, in soils at 0.5 to 4.3%, in streams at an average of roughly 0.7 mg/L, and in groundwater at 0.1 to 10 mg/L. The minerals pyrite, taconite, magnetite, and hematite contain iron. It is extensively used in steel and other alloys. The concentration of carbonate regulates the solubility of ferrous ions (Fe^{+2}). Any soluble iron in groundwater is typically in the ferrous state because it is frequently anoxic. Ferrous iron undergoes oxidation to the ferric state (Fe^{+3}) upon exposure to air or in the presence of oxidants. It may then be hydrolyzed to produce red, insoluble hydrated ferric oxides. Unless the pH is extremely low, ferric iron is not substantially soluble in the absence of complex-forming ions such as phosphate.

In addition to giving meals unpalatable flavors and colours, high iron levels in water can also discolor pipes, clothes, and kitchenware. For irrigation water, the Food and Agriculture Organization of the United Nations recommends a level of 5 mg/L. According to Rice *et al.* [5], the MCL for the secondary drinking water standard set by the US EPA is 0.3 mg/L. The World Health Organization states that 0.3 mg/L is the highest permissible amount of iron [6]. The Ministry of Health and Population determined the maximum allowable value of 0.3 mg/L for iron, which is also the value that Egypt has adopted in its national drinking water regulations. Iron and manganese are

*Corresponding author E-mail: gomaa.ali@ukf.ac.ae, gomaasanad@gmail.com

frequently found in groundwater sources used by different water systems. The presence of manganese and iron in drinking water does not harm human health. However, problems with coloring, staining, turbidity, and unpleasant taste are caused by higher concentrations. Additionally, manganese and iron dioxides build up in pipes [7]. The accumulation of Mn and Fe in distribution systems eventually leads to a reduction in pipe diameter and blockage [8]. The growth of ferruginous and manganese bacteria on pipe walls can be influenced by the iron and Mn content of groundwater.

Many technologies have been developed to remove heavy metals from water, including coagulation [9], chemical precipitation [10], biological operations [11], membrane filtration [12], ion exchange [13], and adsorption [14, 15, 16]. The adsorption process can remove multiple compounds without the need for high temperatures [17, 18, 19, 20, 21]. Numerous adsorbents have been examined in previous studies, such as clays [22], biochar [23, 24], metal oxides [25], chitosan [26], activated carbon [27, 28], and agricultural wastes such as maize stalks [29]. A dark (black) porous solid made mostly of amorphous carbon, biochar is produced as a byproduct of pyrolyzing (i.e., partially burning or heating) biomass materials such as woody residues [30], agricultural byproducts [31], animal bones [32], or other biomass materials (such as sewage sludge and animal manure) with little air flow [33, 34]. Biochar has been thoroughly investigated in the past few decades for its possible use as an environmental remediator and long-lasting soil health enhancer [35]. According to Shan *et al.* [36], biochar is currently regarded as one of the most economical and successful treatment techniques for eliminating heavy metals from soil and water.

It may also serve as a low-cost, environmentally friendly substitute for removing contaminants from water [37, 38, 39]. Biochar's unique characteristics, such as its porous structure, enriched surface functional groups, large specific surface area, and mineral ingredients, enable it to have a high adsorption capacity [40]. Additionally, compared to active AC or other adsorbing materials, BC is less costly and simpler to produce [41]. Biochar shares a porous structure with activated carbon, the most popular and effective sorbent worldwide for eliminating a variety of contaminants from water. Because biochar requires less energy and does not require chemicals or physical activation, it is six times less expensive than activated carbon, making it a promising new low-cost and effective adsorbent [42]. The present study demonstrated the adsorption efficiency of the biochar prepared from COSB to remove Fe(II) from aqueous solutions.

2. Materials and Methods

2.1 Characterization techniques

The nitrogen adsorption–desorption technique (BEL SORP-MAX, Japan) was employed to measure the specific surface area, pore volume, and pore size distribution. An X-ray diffractometer (XRD, PW1710, Philips, Cu-K_α radiation with λ= 1.542 Å) was used to examine the diffraction pattern. From 4° to 70°, the measurement was performed in steps of 0.023°. Fourier transform infrared (FTIR, 400–4000 cm^{-1}) spectroscopy was used to examine the variations in the vibration frequencies of the functional groups of the biosorbent before and after biosorption. Scanning electron microscopy (Zeiss sigma 500 VP FESEM, Germany) was used to examine the changes in the morphological surface of the adsorbents before and after adsorption. The elemental composition of the biochar before and after adsorption was determined using EDX (Zeiss sigma 500 VP FESEM, Germany). A spectrophotometer model DR6000 from Germany was used to determine the amount of Fe(II) present in the supernatant. A pH meter model Orion-4-star from Thermo Scientific in the USA was used to alter the pH. A Velp Scientifica-Italy magnetic stirrer (model F20500011) was used to agitate the adsorption mixture at 300 rpm. A completely automatic single water still type A4000 (Stuart Aquatron) was used to manufacture distilled water.

2.2. Preparation of biochar

The stem of *C. olitorius,* the agricultural waste, used as an adsorbent in this study was obtained from local farmers, rinsed multiple times with tap water, and then with distilled water. Subsequently, it was dried naturally in the sun, broken into small fragments, and ground to achieve smaller dimensions, and then pyrolyzed for 1.25 h at 550 °C in a tube furnace (NEy 2-525 SII, U.S.A) in the absence of oxygen.

2.3 Stock Fe(II) solution

All chemicals and reagents used in this experiment were of certified analytical grade. Stock Fe(II) solution (1000 mg/L prepared by dissolving 4.978 g $FeSO_4.7H_2O$ in distilled water and diluted to 1000 mL), following the method outlined in 3500-Fe B [5].

2.4 Procedure

The batch adsorption system consisted of six 100 ml beakers, each containing 30 mL of Fe(II) solution and 0.03 g of adsorbent (1 g/L). Then, a magnetic stirrer was used to shake the system at 300 rpm to determine the contact time. Each beaker was centrifuged at 2000 rpm for 30 min, and the remaining ferrous ion concentration in the wastewater was determined according to method 3500- Fe-B [5].

3. Results and Discussion

3.1 Characterization of the biosorbent

3.1.1 BET analysis

Fig. 1 shows the N_2 adsorption-desorption isotherm of COSB. The mean pore diameter, total pore volume, and

surface area were measured to be 30.6 nm, 0.675 cm^3/g, and 88.2 m^2/g, respectively. The results indicate that COSB has a significantly greater surface area than other biochars, such as BPB, PBPB, Rice husks, corn straw, and peanut shell biochar. Kim *et al.* [43] reported a specific surface area 11.32 m^2/g, 27.41 m^2/g and total pore volume 0.027 cm^3/g, 0.032 cm^3/g for pristine banana peel biochar (BPB) and phosphoric acid pre-treated biochar (PBPB) respectively. Kizito *et al.* [44] recorded specific surface area 10.995 m^2/g, for biochar made from rice husks. Liu *et al.* [45] recorded specific surface area 4.93 m^2/g and 7.40 m^2/g for biochar made from Corn straw and Peanut shell, respectively. Amer *et al.* [46] reported surface area 16.7341 m^2/g for activated carbon made from rice husk. Özçimen *et al.* [47] reported a specific surface area of 11.2474 m^2/g, 14.6836 m^2/g, 14.4770 m^2/g, 0.6717 m^2/g and total pore volume 0.1847 ml/g, 0.1250 ml/g, 0.1643 ml/g, 0.1842 ml/g for apricot stone biochar, hazelnut shell biochar, grapeseed biochar and chestnut shell biochar, respectively. The pore volume describes the saturation of the pores with N_2 at the most significant relative pressure (P/Po), where P/Po = 0.95. It is expected that COSB will adsorb more cations because of its larger surface area.

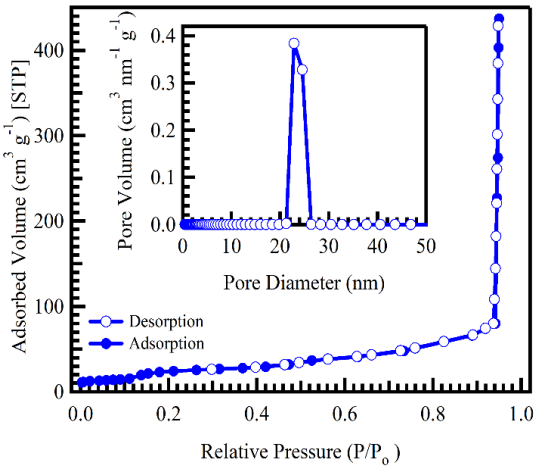

Fig. 1: N_2 adsorption-desorption isotherm of COSB biosorbent.

3.1.2 X-ray diffraction

As seen in Fig. 2, the XRD pattern of COSB shows amorphous aromatic carbon without a crystalline order. A diffraction peak centered at $2\theta \approx 24–26°$, corresponding to a d-spacing of approximately 3.50 Å, was clearly observed. This peak indicates the formation of an aromatic carbon structure during pyrolysis. Additional weak and relatively sharp peaks were observed at d-spacing values of 3.96, 1.97, and 1.73 Å. These peaks are attributed to residual inorganic mineral phases, such as alkaline earth metals, which originate from the natural mineral content of biomass and remain after pyrolysis [48].

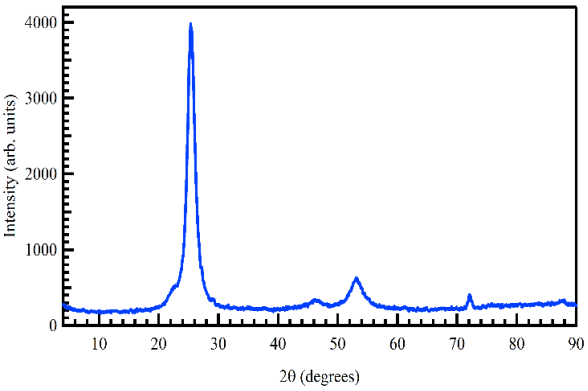

Fig. 2: XRD pattern of COSB biosorbent.

3.1.3 Infrared spectroscopy

The main chemical components of agricultural waste are cellulose, lignin, and hemicellulose. One of the primary components is cellulose, a polysaccharide composed of glucose units. According to Hesas *et al.* [49], the primary functional groups in these units are the anticipated hydroxyl groups, which typically appear around 3500 cm^{-1}, the C-H aliphatic, which typically appears around 2900 cm^{-1}, the C-O band, which appears around 1100 cm^{-1}, and the C=C aromatic, as shown in Table 1. To ascertain the difference in the vibration frequencies of their functional groups, the FTIR spectra of COSB were recorded at 4000-400 cm^{-1} both before and after the biosorption of Fe(II), as shown in Fig. 3. The carbonyl C=O and phenolic -OH groups were altered following the uptake process, as indicated by the changes in their adsorption peaks. It is clear that these groups were involved in the biosorption process, with the adsorbate chemically interacting with the C=O and -OH groups present on the biosorbent surface. According to several studies, the -OH and C=O groups found in several biosorbents are crucial for the adsorption of Fe(II) [43, 50].

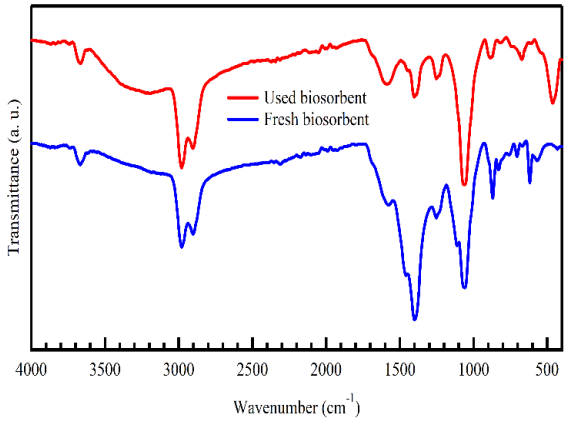

Fig. 3: FTIR analyses of fresh and used COSB biosorbents.

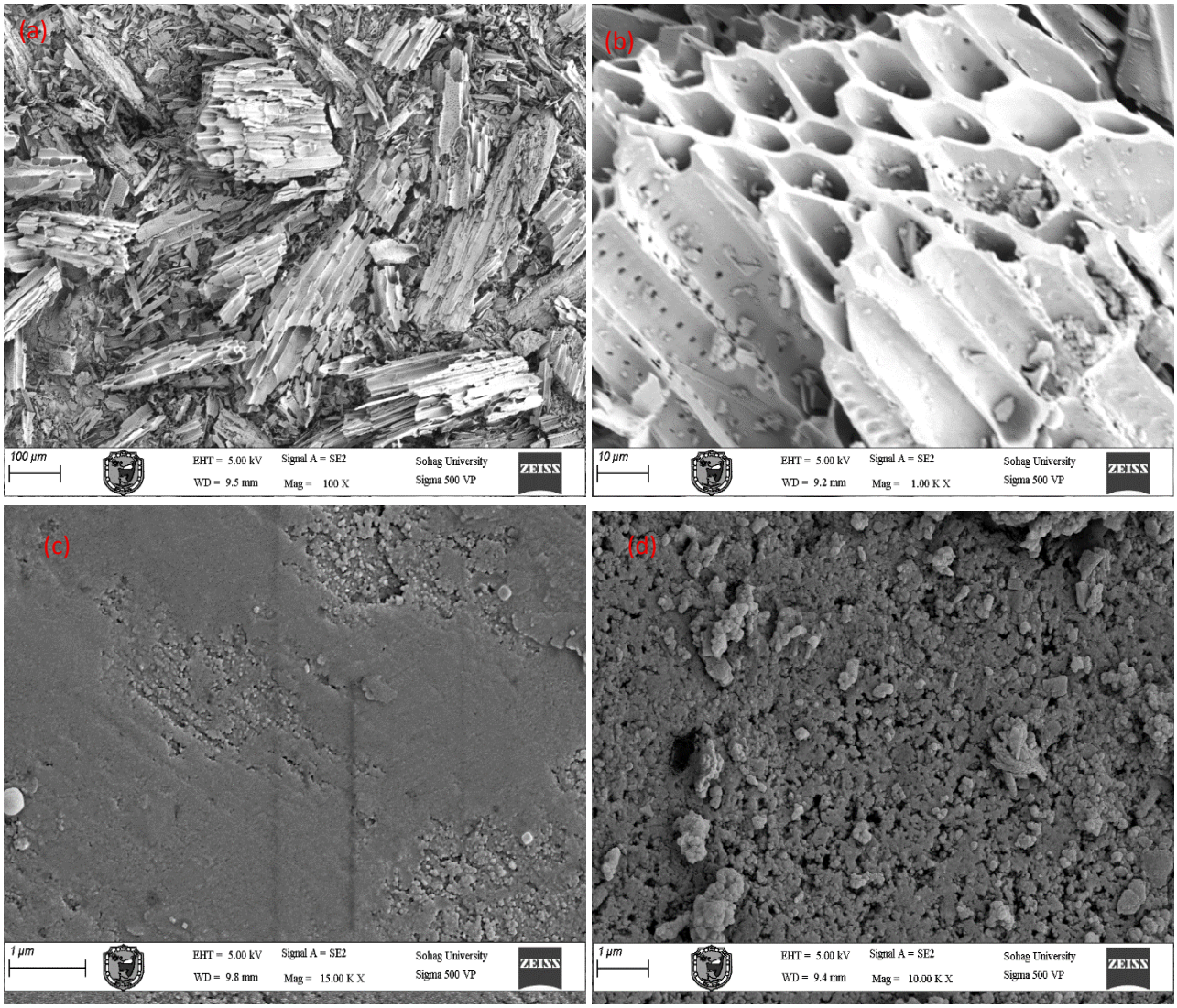

Fig. 4: SEM images of fresh (a, b) and used (c, d) COSB biosorbents.

Table 1: Fundamental FTIR bands of COSB before and after Fe(II) ion biosorption.

FTIR bands	Assignment
3667.15	O–H stretch, H bonded, alcohol,
2979.08 2903.41	C–H stretching vibrations of $–CH_2$ and $–CH_3$ functional group
1577.04 1458.31	C=C ring stretch aromatic C–C stretching
1399.79	C–H aliphatic –CH3 or $–CH_2$
1252.61	C=O stretching of carbonyl group
1110.52	C–OH stretching of phenol
1058.19	C−O stretching vibration of OCH_3 groups
869.89	Aromatic C–H

3.1.4 SEM Morphology

Asymmetric, rough pores and a cylinder-shaped structure prior to the adsorption of Fe(II) ions were observed in the COSB microphotograph, as shown in Fig. 4. The interaction with Fe(II) ions is supported by the coarse surface of the COSB. Furthermore, the SEM images show that following the adsorption of Fe(II) ions, the surface of COSB was smooth, glossy, and had closed pore structures. This is the outcome of a physicochemical interaction between Fe(II) ions and the functional groups on the surface of COSB.

3.1.5 Energy dispersive X-ray analysis

SEM-EDX was performed before and after adsorption (Fig. 5). The results of sample analysis before adsorption confirmed the presence of carbon (64.6), oxygen (17.6), potassium (10.9), calcium (2.9), chloride (1.8), magnesium (0.6), phosphorus (0.6), sulfur (0.6) wt. %, and traces of sodium, as shown in (Fig. 5a). The results indicated that the carbon percentage (64.6 %) was the highest. Sun *et al.* [51]

reported that the biochar made from corn straw, cotton straw, wheat straw and rice straw has a high carbon content with a moderate oxygen content and substantial amounts of potassium, calcium, magnesium, and sodium and the elemental compositions of the biochar are greatly dependent on the source materials. The presence of 11.2% of Fe(II) after adsorption confirmed that COSB is a good adsorbent material for Fe(II) ions (Fig. 5b).

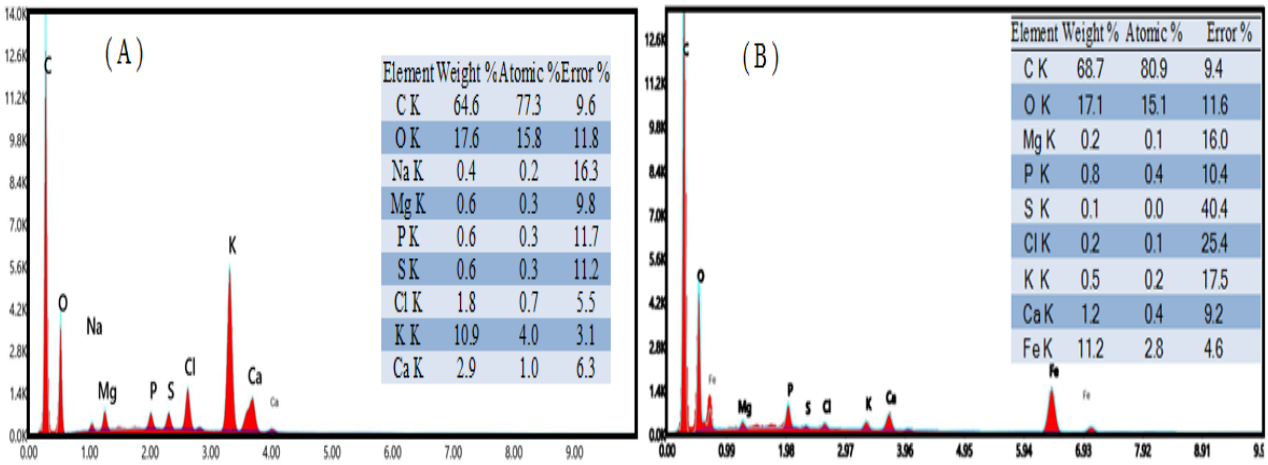

Fig. 5: EDX of COSB: fresh (a) and used (b) biosorbents.

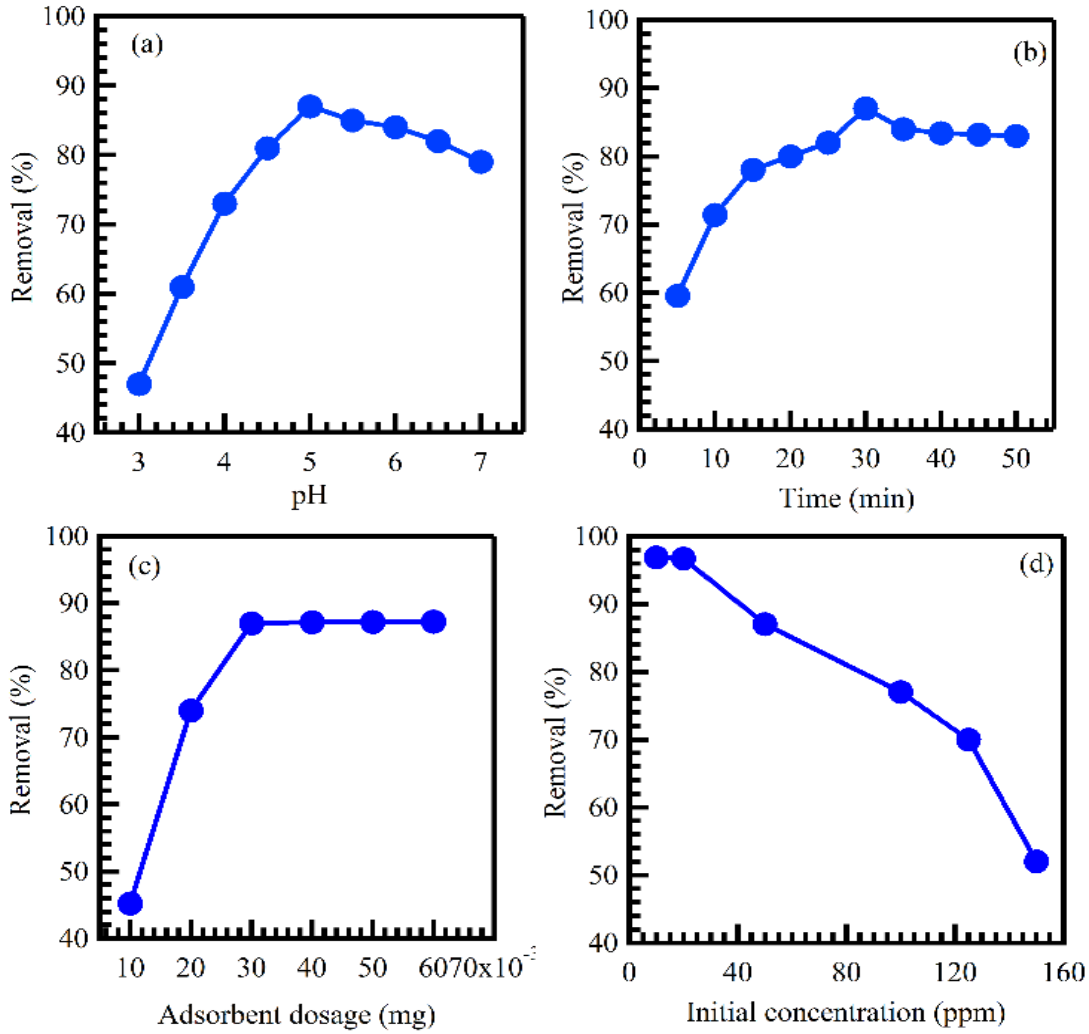

Fig. 6: Influence of pH (a), contact time (b), dosage (c), and initial concentration (d) on Fe(II) ions adsorption on COSB.

3.2 The influence of different factors on Fe(II) ions adsorption by COSB

3.2.1 pH effect

The pH of the solution is a crucial factor in determining the adsorption capacity. Owing to the competing influence of H^+ ions, the ionization of functional groups on the sorbent surface is influenced by the pH of the surrounding solution [52]. The effect of pH on the adsorption of Fe(II) was investigated at room temperature by changing the pH from 3 to 7. As shown in Fig. 6a, the highest removal of Fe(II) (approximately 87.0%) was accomplished at pH 5. The elimination percentage decreased as the pH of the solution decreased. Acidic solutions contain more protons, which effectively compete with Fe(II) to reduce the removal %. Fe(II) precipitated as iron hydroxide at pH values greater than 5, which reduced the removal % [53]. Zhang *et al*. [54] found that the ideal pH for removing Fe(II) using rice husk ash was 5. According to Alslaibi *et al.* [50], activated carbon made from olive stone waste was used to remove 99.39% of Fe(II), 99.32% of Pb^{2+}, and 99.24% of Cu^{2+} at the optimum pH of 5. Elwakeel *et al.* [55] however, found that activated carbon made from sugarcane bagasse had the highest sorption capacity of ferrous and manganous at pH 6.5 ± 0.1.

3.2.2 Influence of contact time

Figure 6b shows that the removal rate increased as time increased, peaking at 30 min. Because there were originally greater surface areas available with free active sites, primarily carboxylic (-COO) and hydroxylic (-OH) groups, adsorption began very quickly and had high removal rates [56]. As contact time increased, the rate at which Fe(II) ions were removed decreased. After 30 min, the system reached equilibrium, and no more Fe(II) could be extracted from the solution because of the saturation of the free active sites, which caused the removal rate to decrease. Abel Uche *et al.* [57] measured the same optimal contact time for the adsorption of Fe(II) ions by watermelon peels. Wan *et al.* [58] investigated the adsorption behavior of aqueous solutions of Fe(II) and Fe(III) ions using chitosan and cross-linked chitosan beads. However, Manel and Béchirm [59] reported that the ideal contact time for removing Fe(II) from artificial groundwater using charcoal as an adsorbent was 20 min. Using chitosan, chitosan-GLA, and chitosan-ECH beads, the contact duration for Fe(II) was 40 min at pH 5, and 60 min for chitosan-EGDE beads at pH 5. However, for Fe(III), chitosan, chitosan-GLA, and chitosan-ECH beads were in contact for 40 min at pH 3, whereas chitosan-EGDE beads were in contact for 60 min at pH 3 [58].

3.2.3 Influence of adsorbent dose

The effect of the adsorbent dosage was examined by adjusting the amount of biochar used from 0.01 to 0.06 g while keeping all other variables constant (Fig. 6c). Because of the increased number of accessible adsorption sites and the increase in adsorbent surface area, increasing the biochar dosage significantly increases the removal rate of Fe(II) [60, 61]. The maximum removal percentage (87.0%) was achieved at 0.03 g. When the dosage exceeded 0.03 g, the adsorption sites aggregated, decreasing the overall adsorbent surface area and, consequently, the removal %. According to Kim *et al.* [43], the pristine and phosphoric acid pre-treated biochar made from banana peels had an adsorbent dosage of 0.1 g/L and 0.3 g/L for Fe(II) removal, respectively, but our work recorded 1 g/L.

3.2.4 Influence of initial Fe(II) concentration

Figure 6d illustrates how various initial Fe(II) concentrations (10, 20, 50,100, 125, and 150 mg/L) were used to study the consequences of initial Fe(II) concentrations on the adsorption rate at room temperature, An increase in the initial Fe(II) concentrations was found to lower the percentage of removal. Above a certain initial Fe(II) concentration, the COSB active sites become saturated, leading to this result. Prior research has documented comparable results [54, 62].

3.3 Adsorption isotherms

Adsorption isotherms describe the interactions between adsorbates and adsorbents, as well as the adsorption process. Four isotherm models, namely Langmuir, Freundlich, Temkin, and D-K isotherms, were used in this investigation.

3.3.1 Langmuir isotherm

According to the Langmuir isotherm theory, a homogenous adsorbent surface with comparable sorption sites is covered by an adsorbate monolayer. According to the Langmuir postulate, there is no transmigration of adsorbate molecules, and the adsorption energy remains constant. The following is the Langmuir adsorption isotherm [63].

$$q_e = \frac{q_m K_L C_e}{1+K_L C_e} \quad (1)$$

where K_L (L/mg) is the Langmuir isotherm constant and q_m (mg/g) is the maximum adsorption capacity. The Langmuir equation can be linearized in the most frequent form as follows [63]:

$$\frac{c_e}{q_e} = \frac{1}{K_L q_m} + \frac{1}{q_m} C_e \quad (2)$$

As shown in Fig. 7a, adsorption of Fe(II) onto COSB at 25 °C is a linear fit using the Langmuir isotherm model. Since R^2 was 0.9907, the Langmuir equation provided a good fit to the adsorption data [19] and it can be mentioned that the adsorption data would follow the Langmuir isotherm, the surface of COSB is homogeneous and the adsorption of Fe(II) formed a monolayer on its outer surface [64]. The Langmuir isotherm has been characterized by the separation factor R_L, which is a dimensionless constant. The R_L factor provides a measure of the adsorption process's favorability [65, 66]. as shown by the following equation:

$$R_L = \frac{1}{1+K_L C_o} \quad (3)$$

where C_o (mg/L) is the highest [Fe(II)]^0. In Table 2, the R_L values, ranging from 0.0166 to 0.2, were found to be less than unity. R_L represents the shape of the isotherm and can be classified as linear (R_L = 1), unfavorable (R_L > 1), favorable (0 < R_L < 1), or irreversible (R_L = 0). The R_L values observed indicate that the adsorption of Fe(II) onto COSB. is a favorable process. Therefore, COSB demonstrates itself as a promising adsorbent for Fe(II).

Table 2: Separation factor at an initial concentration of Fe(II).

C_o (mg/L)	R_L
10	0.2020
20	0.1124
50	0.0482
100	0.025
125	0.0199
150	0.0166

3.3.2 Freundlich isotherm

According to Vijayakumar *et al*. [67] a Freundlich model (Fig. 7b) posits that adsorption takes place on heterogeneous surfaces and that the concentration of adsorbate on an adsorbent surface rise with its concentration. The multilayer adsorption capacity is represented by the Freundlich constant KF (L/mg), while the energy distribution and heterogeneity of the adsorbent sites are represented by the adsorption intensity (1/nF) [68]. The following is the Freundlich equation.

$$Q_e = K_F (C_e)^{1/n} \quad (4)$$

But the linear forms of Freundlich are given as:

$$lnQ_e = lnK_F + \frac{1}{n_F} lnC_e \quad (5)$$

According to Table 3, Freundlich's R^2 value is lower than Langmuir's (0.9907). Thus, the Langmuir model is more relevant to the adsorption of Fe(II) on COSB than the Freundlich model, in contrast to the latter. The value of 0.3924 for $1/n_f$ confirms the adsorption process is favorable but no heterogeneity has been observed (the adsorption is favorable when $0.1 < 1/n_f < 1$).

3.3.3 Temkin isotherms

The Temkin model assesses an adsorbent's ability to adsorb a particular adsorbate. According to this model, the heat of adsorption decreases as the surface coverage increases [69]. The following is an explanation of the Temkin equation.

$$Q_e = \frac{RT}{B_T} \ln (K_T C_e) \quad (6)$$

The Temkin model linearized in common form as follows [16].

$$Q_e = \frac{RT}{B_T} \ln K_T + \frac{RT}{B_T} \ln C_e \quad (7)$$

where T is the absolute temperature of the solution (K), R is the general gas constant (8.314 J/mol·K), K_T is the Temkin isotherm constant related to adsorption capacity (in L/g), and B_T is the Temkin constant related to the heat of sorption (in J/mol). Plotting of the relationship between Q_e and log C_e in Fig. 7c shows a linear association. B_T and K_T have been shown to have values of 0.1716 kJ/mol and 5.75 L/g, respectively. This suggests that the physisorption model predominates in these isothermal investigations. A B_T value below 8 signifies a poor interaction during physisorption, whereas a value above 8 implies a greater amount of chemisorption during the removal of metal ions [70].

3.3.4 Dubinin-Radushkevich Isotherm

According to their mean free energy, this model was frequently used to distinguish between the physical and chemical adsorption of metal ions [71]. When the adsorption energy (E_D) is less than 8.0 kJ/mol, physisorption takes place (Fig. 7d). However, when the E_D is between 8 and 16 kJ/mol, chemisorption takes place [72]. According to Chen *et al.* [1] the Dubinin-Radushkevich model can be used to both homogeneous and heterogeneous surfaces. The following is one way to express the Dubinin-Radushkevich equation:

$$Q_e = q_s e^{-k_D \varepsilon^2} \quad (8)$$

The linear form of the Dubinin-Radushkevich model is given as:

$$lnq_e = lnq_s - k_D \varepsilon^2 \quad (9)$$

The DR monolayer capacity constant is represented by q_s (mg/g), K_D (Mol^2/K·J^2) is the DR constant associated with adsorption energy, and ε (KJ^2 Mol^{-2}) represents Polanyi's potential, which is connected to the free energy of adsorption. The E_D can be calculated from the following eq.:

$$E_D = \frac{1}{\sqrt{2K_D}} \quad (10)$$

The results of the E_D calculation are shown in Table 3; the value is 1.75 kJ/mol confirms physisorption. This means that adsorption of one mole of Fe(II) ions from an infinitely dilute solution onto the surface of COSB. requires a free energy change of 1.75 kJ/mol. Zhang *et al*. [54] reported E_D equals 2.53 kJ/mol for adsorption of Fe(II) on Rice Husk Ash.

The adsorption capacity of COSB for Fe(II) was compared with various other adsorbents, as summarized in Table 4. The results demonstrate that COSB possesses a superior maximum monolayer adsorption capacity (83.33 mg/g) compared to other materials such as rice husk ash, maize stalks, and various chitosan-based beads, confirming its high efficiency as a cost-effective biosorbent.

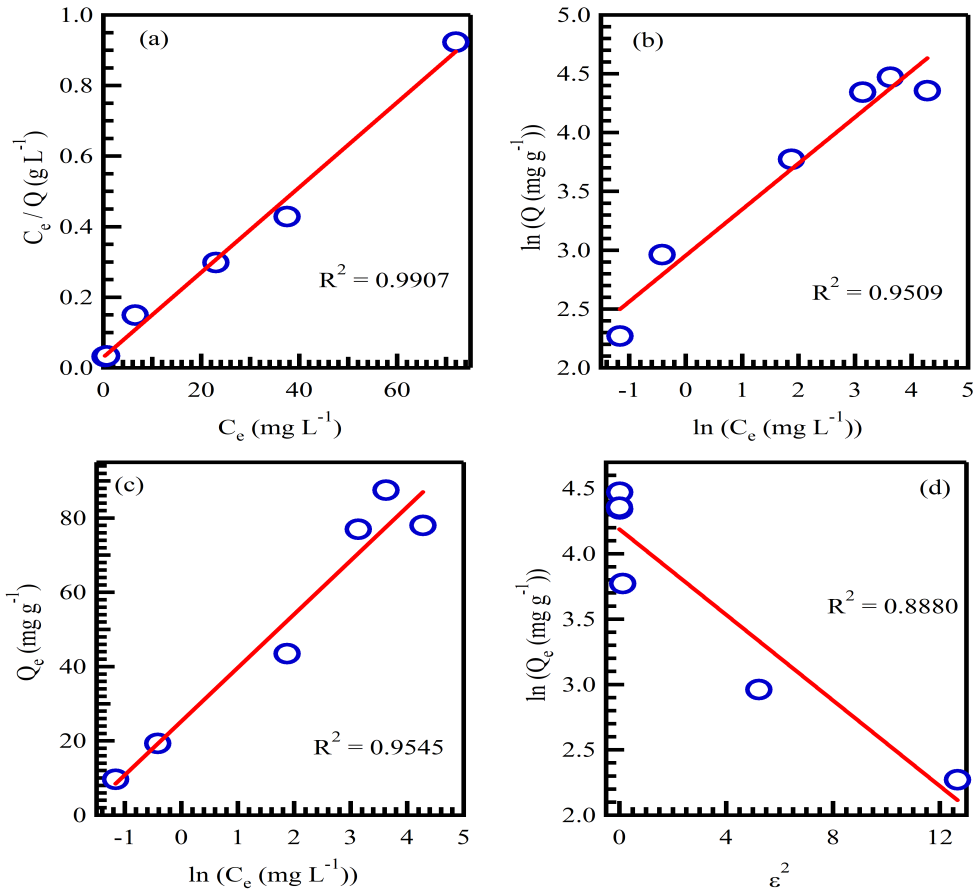

Fig. 7: Linear form of sorption isotherm for Fe(II) adsorption onto adsorption on COSB, Langmuir (a), Freundlich (b), Temkin (c), and Dubinin–Radushkevich (d).

Table 3: Langmuir, Freundlich, Temkin, and Dubinin-Radushkevich constants for the adsorption of Fe(II) onto COSB. (T = 298 K, time= 30 min, Initial concentration of Fe(II) = 50 mg/L, pH = 5, volume of solution = 0.03 L, dosage = 0.03 g.

Langmuir			**Freundlich**			**Temkin**			**Dubinin-Radushkevich**			
Q_m (mg/g)	K_L (L/mg)	R^2	$1/n_F$	K_F (L/mg)	R^2	K_T (L/g)	B_T (kJ/mol)	R^2	Q_s (mg/g)	K_D ($mol^2/K.J^2$)	E_D (kJ/mol)	R^2
83.33	0.395	0.9907	0.3924	19.21	0.9509	5.75	0.1716	0.9454	65.923	0.1638	1.747	0.8880

Table 4: Comparison of adsorption capacities of different adsorbents for ferrous ions.

Adsorbent	**Adsorption capacity (mg/g)**	**Contact time (min)**	**C_o (mg/L)**	**pH**	**Reference**
Coir fibres	2.84	120	73.50–444.8	5	[73]
Maize stalks	5.14	75	10-40	6	[29]
Rice husk ash	6.21	60	2–40	5	[54]
Modified coir fibres	7.49	120	73.50–444.8	5	[73]
Chitosan-EGDE	38.61	60	3-9	5	[58]
Chitosan	64.1	40	3–9	5	[58]
Olive stone activated carbon (OSAC)	57.47	120	20	5	[50]
Chitosan-ECH beads	57.47	40	3-9	5	[58]
COSB	83.33	30	10-150	5	This work

Table 5: Kinetic parameters for the adsorption of Fe(II) ions onto COSB.

Pseudo First Order				Pseudo Second Order			Elovich				Intraparticle diffusion		
q_e, exp (mg/g)	q_e, cal (mg/g)	k_1 (min^{-1})	R^2	q_e, cal (mg/g)	K_2 (g/mg.min)	R^2	t_o min	a (g/mg.min)	b (g/mg)	R^2	k_p (mg/g. $min^{1/2}$)	C (mg/g)	R^2
43.5	18.73	0.0841	0.9726	47.17	0.007	0.9977	0.08	94.26	0.138	0.9824	3.9215	22.336	0.9490

3.4 Adsorption kinetic models

The interaction between the adsorbent and the adsorbate at a specific time can be explained by the adsorption kinetic model. It is helpful in figuring out the best order for the pseudo-kinetic models and learning more about the adsorption process (physisorption or chemisorption) [74]. Three models were used in this study: the Elovich model [75], the pseudo-second-order [76], and the pseudo-first-order [77].

3.4.1 Pseudo-first-order equation

Lagergren's relation provides the following pseudo-first-order model [78]:

$$q_t = q_e(1 - e^{-K_1 t}) \quad (11)$$

where k_1 is the rate constant of adsorption (min^{-1}), q_t represents the amount adsorbed at time t (min), and q_e represents the amount of Fe(II) adsorbed (mg/g) at equilibrium.

The linearized form of the PFO model is as follows.

$$\ln(q_e - q_t) = \ln q_e - K_1 t \quad (12)$$

The slope and intercept of the $\ln(q_e - q_t)$ vs. t plots were used to calculate the k_1 and q_e values.

The results in Fig. 8a and Table 5 confirm the R^2 value is not the highest value and the poor agreement between the experimental and calculated q_e values. This reveals that the kinetics of Fe(II) ions adsorption onto COSB do not follow the first order.

3.4.2 Pseudo-second-order equation

The pseudo-second-order equation was given by Ho and McKay [79]. Eq. 14 is the nonlinear form of the PSO model.

$$q_e = \frac{q_e^2 k_2 t}{q_e k_2 t + 1} \quad (13)$$

The most widely used linearized form of PSO can be represented as in Eq. 14.

$$\frac{t}{q_e} = \frac{1}{q_e^2 k_2} + \frac{1}{q_e} t \quad (14)$$

where the pseudo-second-order adsorption rate constant is denoted by k_2 (g/mg.min). We can calculate the values of q_e and k_2 from the plot of t/q_t vs. t in Fig. 8b. Table 5 shows that there is good agreement between the calculated and experimental q_e values, and the R^2 values are very high. Consequently, the adsorption of Fe(II) onto COSB is well described by pseudo-second-order kinetics. Similar patterns were observed in the adsorption kinetics of Fe(II) ions onto BPB and PBPB [43].

3.4.3 Elovich model

Chemical adsorption has made extensive use of the Elovich equation [75]. When the adsorbing surface is heterogeneous, the Elovich equation is frequently true [80]. The adsorption of pollutants from aqueous solutions has been well characterized in recent years by Elovich's equation [81, 82].

Elovich's equation is as follows:

$$q_t = \frac{1}{b} ln(\mathrm{t} + t^o) - \frac{1}{b} ln(t^o) \quad (15)$$

where $t^0 = 1/ab$, If $t >> t^0$, the equation can be simplified to the linearized form as follows:

$$q_t = \frac{1}{b} ln(\mathrm{t}) - \frac{1}{b} ln(ab) \quad (16)$$

where the value 1/b (mg/g) is associated with the availability of adsorption sites, and 'a' indicates the initial adsorption rate (mg/g.min). A linear relationship is obtained by plotting qt versus ln(t), as shown in Fig. 8c. The values of a = 94.26 (mg/g.min) and 1/b = 7.24 (mg/g) were derived from the line's intercept and slope. These and the other factors are summarized in Table 5. The pseudo-second-order model fits the experimental data and the best out of all the models that were taken into consideration.

3.4.4 Intraparticle diffusion model

The solute intraparticle diffusion in adsorbents is explained using the Weber-Morris model [83], which is expressed as [84]:

$$q_t = k_p t^{1/2} + C \quad (17)$$

where C (mg/g) is the intercept of the plot of q_t vs. $t_{0.5}$, which indicates the thickness of the boundary layer. According to Kannan and Sundaram. [85], the larger the intercept, the greater is the boundary layer effect, and k_p is the intraparticle diffusion rate constant (mg/g.$min^{1/2}$), determined from the slope. A straight line that does not pass through the origin (Fig. 8d) signifies that pore diffusion is the main factor affecting sorption. According to Sujana and Mohanty [86], this implies that solute ions diffuse within the adsorbent material's pores and capillaries. The film diffusion process is thought to be the rate-limiting stage, if the plot ceases to be linear, as shown in Fig. 8d.

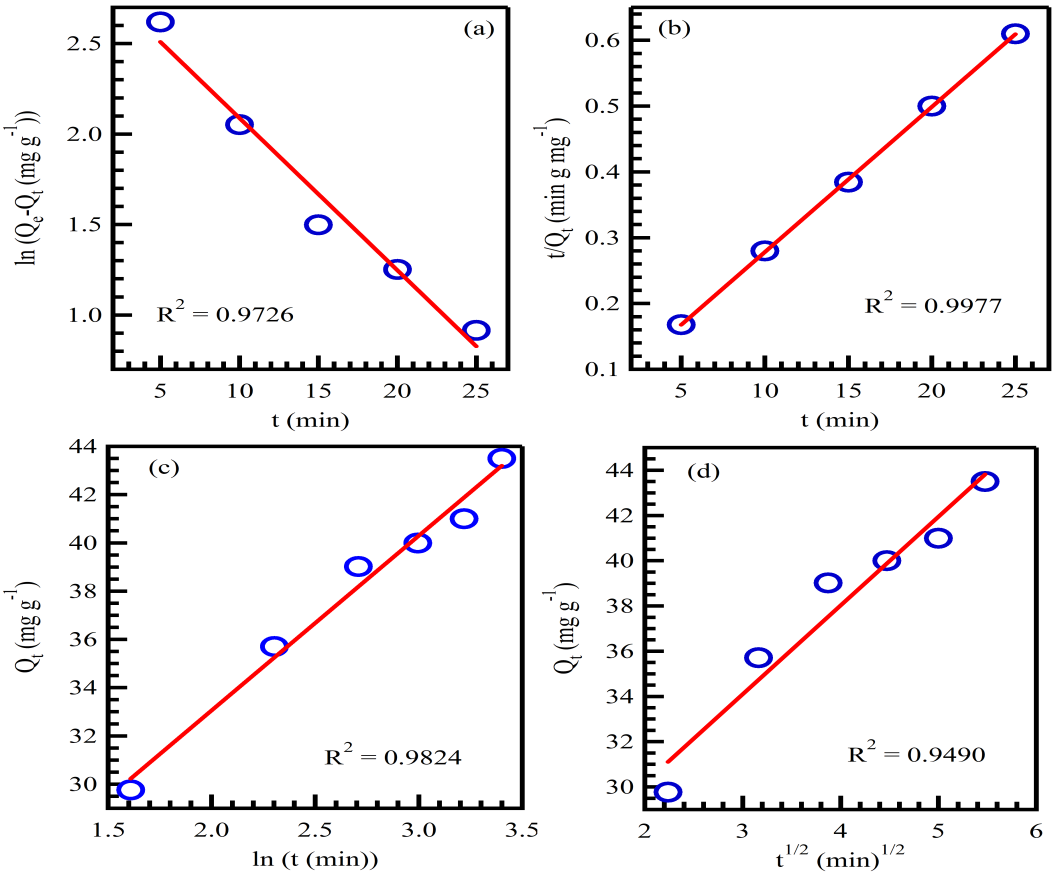

Fig. 8: Kinetic curves for pseudo-first-order (a), pseudo-second-order (b), simple Elovich (c), and intraparticle diffusion (d) models for Fe(II) adsorption onto COSB.

3.5 Adsorption thermodynamics

Entropy change (ΔS°), enthalpy change (ΔH°), and free energy change (ΔG°) are examples of thermodynamic data that can be used to better understand the adsorption process. The kind of adsorption (chemisorption or physisorption), process type (endothermic or exothermic), and adsorption mechanism can all be better understood by examining these factors. The relationship between temperature and equilibrium constant is described by the Van't Hoff equation, which is expressed as follows.

$$\Delta G° = -RT \ln Ke^{\circ} \quad (18)$$

$$\Delta G° = \Delta H° - T\,\Delta S° \quad (19)$$

$$ln K_e{}^{o} = \frac{\Delta H^{o}}{RT} + \frac{\Delta S^{o}}{T} \quad (20)$$

where Ke° is the thermodynamic equilibrium constant, R is the general gas constant J/mol.K, and T is the absolute temperature in Kelvin (K). Plotting ln (Ke°) versus 1/T and taking the intercept will get the entropy change (ΔS°). The enthalpy change (ΔH°) can also be found by looking at the slope of the plot. The following formula is used by Lima *et al.* to calculate the thermodynamic equilibrium constant (Ke°) [87].

$$K_e{}^{o} = \frac{1000 x kg x Mw x [Adsorbate]^{o}}{\gamma} \quad (21)$$

In the given context, γ stands for the dimensionless coefficient of activity, MW for the adsorbate's molecular weight (g/mol), kg (L/mg) for the adsorption constant for the Langmuir isotherm (the best-fitting isotherm in the study that is being presented), and [Adsorbate]° for the adsorbate's standard concentration (1 mol/L). It is assumed that if the adsorbate solution is sufficiently diluted, we can take the activity coefficient to be unity. Table 6 displays all of the thermodynamic parameters. The endothermic nature of Fe(II) adsorption on COSB is indicated by the positive ΔH° value. The positive value of ΔS° indicates that the entropy increased at the solid/solution interface. The negative ΔG° value indicates that the adsorption of Fe(II) ions onto COSB is favorable and spontaneous. Elwakeel *et al.* [55] reported the same outcome for the adsorption of Fe(II) onto activated carbon made from sugarcane bagasse. Adsorption processes with ΔG° values between -20 and 0 kJ/mol are associated with spontaneous physical processes, whereas chemisorption is associated with values between -80 and -400 kJ/mol [88, 89, 90]. Regarding this system, there is a physisorption process shown by the ΔG° values, which range from -24.77 to -27.69 kJ/mol. Chemical or physical sorption is also determined by the enthalpy of a sorption process.

Enthalpy values range from 8 to 25 kJ/mol for physical sorption and from 83 to 830 kJ/mol for chemical sorption [88]. It can be concluded from the low values of ΔH° (18.76) that the interaction between Fe(II) and biochar is physical sorption.

Table 6: Calculated thermodynamic parameters for Fe(II) adsorption on COSB.

T (K)	K_e (L/mg)	K_e^o	Ln K_e^o	ΔG° (kJ/mol)	ΔH° (kJ/mol)	ΔS° (J/mol.K)
298	0.395	22044.1	10.0008	-24.77	18.76	146.1
308	0.5	27922.5	10.24	-26.23		
318	0.635	35473.87	10.476	-27.69		

4. Conclusion

This work investigated the possibility of utilizing COSB as a practical, secure, and affordable material to extract Fe(II) from aqueous solutions. BET analysis shwoed high surface area of 88.2 m^2/g, pore diameter of 30.6 nm, with a total pore volume of 0.675 cm^3/g. XRD, SEM, and EDX studies confirmed the adsorption of ferrous ions on the COSB, whereas FTIR analysis illustrated the crucial roles that hydroxyl and carboxyl groups play in the adsorption process. The experimental data demonstrated high applicability to the Langmuir model with a maximum saturated monolayer sorption capacity of 83.33 mg/g, and equilibrium isotherms indicated that the ideal adsorption conditions were pH 5, adsorbent dosage 1 g/L, and contact time 30 minutes at 298 K. The kinetic investigations conducted in this work showed that the data follow the pseudo-second-order model R^2 (0.9977). The sorption process is endothermic with a positive entropy value. The positive value of ΔS° suggests an increase in randomness at the solid/solution interface. The negative Gibbs' free energy values (ΔG°) validate the process's spontaneous character. This indicates that the Fe(II) can be effectively removed from wastewater by using COSB.

References

[1] Chen, Y.; Shinogi, Y.; Taira, M. (2010) Influence of biochar use on sugarcane growth, soil parameters, and groundwater quality. Soil Research 48, 526.

[2] Edokpayi, J. N.; Enitan, A. M.; Mutileni, N.; Odiyo, J. O. (2018) Evaluation of water quality and human risk assessment due to heavy metals in groundwater around Muledane area of Vhembe District, Limpopo Province, South Africa. Chemistry Central Journal 12, 2.

[3] Viotti, P.; Marzeddu, S.; Antonucci, A.; Décima, M. A.; Lovascio, P.; Tatti, F.; Boni, M. R. (2024) Biochar as an alternative material for heavy metal adsorption from groundwaters: lab-scale (column) experiment review. Materials 17, 809.

[4] Uwamarriya, V. (2013) Adsorptive Removal of Heavy Metals from Groundwater by Iron Oxide Based Adsorbents. UNESCO-IHE Institute for Water Education (Netherlands).

[5] Baird, R.B.; Eaton, A.D.; Rice, E. W. (2017) Standard methods for the examination of water and wastewater, 23rd edition. American Public Health Association, Washington DC, USA.

[6] World Health Organization (WHO) (2004) Guidelines for Drinking Water Quality. World Health Organization 1.

[7] Dalai, C.; Jha, R.; Desai, V. R. (2015) Rice husk and sugarcane bagasse-based activated carbon for iron and manganese removal. Aquatic Procedia 4, 1126-1133.

[8] Tekerlekopoulou, A. G.; Vayenas, D. V. (2007) Ammonia, iron, and manganese removal from potable water using trickling filters. Desalination 210, 225-235.

[9] Yao, W.; Wang, J.; Wang, P.; Wang, X.; Yu, S.; Zou, Y.; Hou, J.; Hayat, T.; Alsaedi, A.; Wang, X. (2017) Synergistic coagulation of GO and secondary adsorption of heavy metal ions on Ca/Al layered double hydroxides. Environmental Pollution 229, 827-836.

[10] Chen, Q.; Yao, Y.; Li, X.; Lu, J.; Zhou, J.; Huang, Z. (2018) Comparison of heavy metal removals from aqueous solutions by chemical precipitation and characteristics of precipitates. Journal of Water Process Engineering 26, 289-300.

[11] Abo-Alkasem, M.I.; Hassan, N.H.; Abo Elsoud, M.M. (2023) Microbial bioremediation as a tool for the removal of heavy metals. Bulletin of the National Research Centre 47, 31.

[12] Al-Rashdi, B. A. M.; Johnson, D. J.; Hilal, N. (2013) Removal of heavy metal ions by nanofiltration. Desalination 315, 2-17.

[13] Benítez, P.; Castro, R.; Barroso, C. G. (2002) Removal of iron, copper, and manganese from white wines through ion exchange techniques: effects on their organoleptic characteristics and susceptibility to browning. Analytica Chimica Acta 458, 197-202.

[14] Maazinejad, B.; Mohammadnia, O.; Ali G.A.M.; Makhlouf A.S.H.; Nadagouda, M.N.; Sillanpää, M.; Asiri A.M.; Agarwal, S.; Gupta, V.K.; Sadegh, H. (2020) Taguchi L9 (34) orthogonal array study based on methylene blue removal by single-walled carbon nanotubes-amine: Adsorption optimization using the experimental design method, kinetics, equilibrium and

thermodynamics. Journal of Molecular Liquids 298, 112001.

[15] Nassar, N. N. (2010) Rapid removal and recovery of Pb (II) from wastewater by magnetic nanoadsorbents. Journal of Hazardous Materials 184, 538-546.

[16] Youssef, A. M.; El-Nabarawy, T.; Samra, S. E. (2004) Sorption properties of chemically-activated carbons: 1. Sorption of cadmium (II) ions. Colloids and Surfaces A: Physicochemical and Engineering Aspects 235, 153-163.

[17] Ali, G. A.; Barhoum, A.; Gupta, V. K.; Nada, A. A.; El-Maghrabi, H. H.; Kanthasamy, R.; Shaaban, E.R.; Algarni, H.; Chong, K. F. (2020) High surface area mesoporous silica for hydrogen sulfide effective removal. Current Nanoscience 16, 226-234.

[18] Agarwal, S.; Sadegh, H.; Monajjemi, M.; Hamdy, A. S.; Ali, G. A.; Memar, A. O.; Shahryari-ghoshekandi, R.; Tyagi, I.; Gupta, V. K. (2016) Efficient removal of toxic bromothymol blue and methylene blue from wastewater by polyvinyl alcohol. Journal of Molecular Liquids 218, 191-197.

[19] Gupta, V.K.; Agarwal, S.; Sadegh, H.; Ali, G.A.M.; Bharti, A.K.; Hamdy, A.S. (2017) Facile route synthesis of novel graphene oxide-β-cyclodextrin nanocomposite and its application as adsorbent for removal of toxic bisphenol A from the aqueous phase. Journal of Molecular Liquids 237, 466–472.

[20] Shayegan, H.; Ali, G.A.; Safarifard, V. (2020) Amide-functionalized metal–organic framework for high efficiency and fast removal of Pb (II) from aqueous solution. Journal of Inorganic and Organometallic Polymers and Materials 30, 3170-3178.

[21] Abd-Ellatif, A.A.I.; Rashed, M. N.; Raslan, M. A. M.; Ali, S.G.A.; Ali, G. A. M. (2024) Cost-effective biosorption of ammonium ion from aqueous solutions using Corchorus olitorius L. leaves. Egyptian Journal of Chemistry 67(6), 95-104.

[22] Abd-Elshafi, A.A.; Amer, A.A.; El-Shater, A.; Newair, E.F.; Elrouby, M. (2023) Organo-modified Montmorillonite-based adsorbents for selective removal of Iron(II) from aqueous solutions. Journal of Molecular Liquids 383, 122092.

[23] Zainab M.; El Hanandeh, A.; Yu, Q. J. (2019) Preparation, characterization and application of surface modified biochar from date seed for improved lead, copper, and nickel removal from aqueous solutions. Journal of Environmental Chemical Engineering 7, 103379.

[24] Zeng, B.; Xu, W.; Khan, S. B.; Wang, Y.; Zhang, J.; Yang, J.; Su, X.; Lin, Z. (2021) Preparation of sludge biochar rich in carboxyl/hydroxyl groups by quenching process and its excellent adsorption performance for Cr (VI). Chemosphere 285, 131439.

[25] Biela, R.; Kučera, T. (2016) Efficacy of sorption materials for nickel, iron, and manganese removal from water. Procedia Engineering 162, 56-63.

[26] Ashraf, A.; Dutta, J.; Farooq, A.; Rafatullah, M.; Pal, K.; Kyzas, G. Z. (2024) Chitosan- based materials for heavy metal adsorption: Recent advancements, challenges and limitations. Journal of Molecular Structure 1309, 138225.

[27] Habeeb O.A.; Ramesh K.; Ali G.A.M.; Yunus R.M. (2017) Lowcost and eco-friendly activated carbon from modified palm kernel shell for hydrogen sulfide removal from wastewater: adsorption and kinetic studies. Desalination and Water Treatment 84, 205-214.

[28] Akl, M. A.; Yousef, A. M.; AbdElnasser, S. (2013) Removal of iron and manganese in water samples using activated carbon derived from local agro-residues. Journal of Chemical Engineering & Process Technology 4, 1-10.

[29] El-Sayed, G. O.; El-Sheikh, R.; Farag, N. H. (2015) Maize stalks as a cheap biosorbent for the removal of Fe(II) from aqueous solution. International Research Journal of Pure and Applied Chemistry 6, 66.

[30] Shaheen, S. M.; Niazi, N. K.; Hassan, N. E.; Bibi, I.; Wang, H.; Tsang, D.C.W.; Ok, Y.S.; Bolan, N.; Rinklebe, J. (2019) Wood-based biochar for the removal of potentially toxic elements in water and wastewater: a critical review. International Materials Reviews 64, 216-247.

[31] He, Z.; Uchimiya, S. M.; Guo, M. (2016) Production and characterization of biochar from agricultural by-products: overview and use of cotton biomass residues. In Agricultural and Environmental Applications of Biochar: Advances and Barriers (eds M. Guo, Z. He and S.M. Uchimiya) 63-86.

[32] Vassilev, N.; Martos, E.; Mendes, G.; Martos, V.; Vassileva, M. (2013) Biochar of animal origin: a sustainable solution to the global problem of high-grade rock phosphate scarcity? Journal of the Science of Food and Agriculture 93, 1799-1804.

[33] Chen Y.-D.; Wang R.; Duan X.; Wang S.; Ren N.-Q.; Ho S.-H. (2020) Production, properties, and catalytic applications of sludge derived biochar for environmental remediation. Water Research 187, 116390.

[34] He, Z. (2012) Applied research in animal manure: Challenges and opportunities beyond the adverse environmental concerns. Nova Science Publishers.

[35] Guo M.; Uchimiya S.M.; He Z. (2016) Agricultural and environmental applications of biochar: advances and

barriers. Soil Science Society of America 63, 495–504.

[36] Shan, R.; Shi, Y.; Gu, J.; Wang, Y.; Yuan, H. (2020) Single and competitive adsorption affinity of heavy metals toward peanut shell-derived biochar and its mechanisms in aqueous systems. Chinese Journal of Chemical Engineering 28, 1375-1383.

[37] Dai, Y.; Zhang, N.; Xing, C.; Cui, Q.; Sun, Q. (2019) The adsorption, regeneration and engineering applications of biochar for removal organic pollutants: a review. Chemosphere 223, 12–27.

[38] Nham, N. T.; Al Tahtamouni, T. M.; Nguyen, T. D.; Huong, P. T.; Jitae, K.; Viet, N. M.; Noi, N.V.; Phuong, N.M.; Anh, N. T. H. (2019) Synthesis of iron-modified rice straw biochar toward arsenic from groundwater. Materials Research Express 6, 115528.

[39] Khorram, M. S.; Zhang, Q.; Lin, D.; Zheng, Y.; Fang, H.; Yu, Y. (2016) Biochar: a review of its impact on pesticide behavior in soil environments and its potential applications. Journal of Environmental Sciences 44, 269-279.

[40] Hussin, F.; Aroua, M. K.; Szlachta, M. (2022) Biochar derived from fruit by-products using the pyrolysis process for the elimination of Pb (II) ion: An updated review. Chemosphere 287, 132250.

[41] Xie, T.; Reddy, K. R.; Wang, C.; Yargicoglu, E.; Spokas, K. (2015) Characteristics and applications of biochar for environmental remediation: a review. Critical Reviews in Environmental Science and Technology 45, 939-969.

[42] Tan, X.; Liu, Y.; Zeng, G.; Wang, X.; Hu, X.; Gu, Y.; Yang, Z. (2015) Application of biochar for the removal of pollutants from aqueous solutions. Chemosphere 125, 70-85.

[43] Kim H.; Ko R. A.; Lee S.; Chon K. (2020) Removal Efficiencies of Manganese and Iron Using Pristine and Phosphoric Acid Pre-Treated biochar Made from Banana Peels. Water 12, 1173.

[44] Kizito, S.; Wu, S.; Kirui, W.K.; Lei, M.; Lu, Q.; Bah, H.; Dong, R. (2015) Evaluation of slow pyrolyzed wood and rice husks biochar for adsorption of ammonium nitrogen from piggery manure anaerobic digestate slurry. Science of the Total Environment 505, 102-112.

[45] Liu, N.; Sun, Z.; Wu, Z.; Zhan, X.; Zhang, K.; Zhao, E.; Han, X. (2013) Adsorption Characteristics of Ammonium Nitrogen by Biochar from Diverse Origins in Water. Advanced Materials Research 664, 305-312.

[46] Amer, A. A.; Elewa, A. M.; Attallah, M. F.; Gad, H. A. (2021) Removal of Some Heavy Metals Contaminants from Aqueous Solutions by Applying Biomass-Based Modified Activated Carbon. Egyptian Journal of Chemistry 64, 5929 – 5944.

[47] O¨zçimen, D.; Ersoy-Meriçboyu, A. (2010) Characterization of biochar and bio-oil samples obtained from carbonization of various biomass materials. Renewable Energy 35, 1319–1324.

[48] Abdulrazzaq, H.; Jol, H.; Husni, A.; Abu-Bakr, R. (2014) Characterization and stabilization of biochar obtained from empty fruit bunch, wood, and rice husk. Bioresources 9, 2888-2898.

[49] Hesas R.H.; Arami-Niya A.; Wan Daud W.M.A.; Sahu J. (2013) Preparation and characterization of activated carbon from apple waste by microwave-assisted phosphoric acid activation: Application in methylene blue adsorption. Bioresources 8, 2950-2966.

[50] Alslaibia, T.M; Abustana, I.; Ahmad, M.A, Abu Foul, A. (2014) Kinetics and equilibrium adsorption of Fe(II), lead (II), and copper (II) onto activated carbon prepared from olive stone waste. Desalination and Water Treatment 52, 7887–7897.

[51] Sun, J.; Lian, F.; Liu, Z.; Zhu, L.; Song, Z. (2014) biochar derived from various crop straws: Characterization and Cd(II) removal potential. Ecotoxicology and Environmental Safety 106, 226–231.

[52] Marañón, E.; Ulmanu, M.; Fernández, Y.; Anger, I.; Castrillón, L. (2006) Removal of ammonium from aqueous solutions with volcanic tuff. Journal of Hazardous Materials 137, 1402-1409.

[53] Taffarel, S.R.; Rubio, J. (2009) On the removal of Mn2+ ions by adsorption onto natural and activated Chilean zeolites. Minerals Engineering 22, 336–343.

[54] Zhang Y.; Zhao J.; Jiang Z.; Shan D.; Lu Y. (2014) Biosorption of Fe(II) and Mn(II) Ions from Aqueous Solution by Rice Husk Ash. BioMed Research International 973095.

[55] Elwakeel K.Z.; El-Sayedb G.O.; Abo El-Nassr, S.M. (2015) Removal of ferrous and manganous from water by activated carbon obtained from sugarcane bagasse. Desalination and Water Treatment 55(2), 471-483.

[56] Sulyman, M.; Namiesnik, J.; Gierak, A. (2017) Low-cost Adsorbents Derived from Agricultural By-products/Wastes for Enhancing Contaminant Uptakes from Wastewater: A Review. Polish Journal of Environmental Studies 26, 479-510.

[57] Abel Uche A.; Bilyamin I.; Timothy M.A.; Raphael O. (2019) removal of Lead (II) and Fe(II) ions from Aqueous Solutions Using Watermelon (Citrillus Lanatus) Peels as Adsorbent. Open Access Journal of Chemistry 3, 1-7.

[58] Wan Ngah. W.S; Ghani. S. Ab; Kamari. A. (2005) Adsorption behaviour of Fe(II) and Fe(III) ions in aqueous solution on chitosan and cross-linked chitosan beads. Bioresource Technology 96, 443–450.

[59] Manel R.; Béchir Ben. (2015) Removal of iron from artificial groundwater by adsorption on charcoal. International Journal of Scientific Research, Engineering Technology 3, 133-137.

[60] Ismail, Z.Z.; Hameed, B.B. (2014) Recycling of raw corn cob residues as an agricultural waste material for ammonium removal: kinetics, isotherms, and mechanisms. International Journal of Environment and Waste Management 13, 217-230.

[61] Sulyman, M.; Namieśnik, J.; Gierak, A. (2014) Utilization of New Activated Carbon Derived from Oak Leaves for Removal of Crystal Violet from Aqueous Solution. Polish Journal of Environmental Studies 23, 2223-2232.

[62] Awad, H.E.; Mohammad, A.M.; Farahat, E.A. (2023) Potential use of dry powder of Vossia cuspidata (Roxb.) Griff. Rhizomes and leaves in methylene blue dye remediation. Scientific Reports 13, 11073.

[63] Al-Ansari. S.H.; Gomaa. H.; Abdel-Rahim. R.D.; Ali. G.A.M.; Nagiub. A.M. (2024) Recycled gold-reduced graphene oxide nanocomposite for efficient adsorption and photocatalytic degradation of crystal violet. Scientific Reports 14, 4379.

[64] Surovka, D.; Pertile, E. (2017) Sorption of iron, manganese and copper from aqueous solution using orange peel: Optimization, isotherm, kinetic and thermodynamic studies. Journal of Environmental Studies 26, 795-800.

[65] Bhattacharyya, K.G.; Sharma, A. (2004) Adsorption of Pb (II) from aqueous solution by Azadirachta indica (Neem) leaf powder. Journal of Hazardous Materials 113, 97-109.

[66] Elmorsi, T.M. (2011) Equilibrium isotherms and kinetic studies of removal of methylene blue dye by adsorption onto miswak leaves as a natural adsorbent. Journal of Environmental Protection 2, 817.

[67] Vijayakumar, G.; Tamilarasan, R.; Dharmendirakumar, M. (2012) Adsorption, Kinetic, Equilibrium and Thermodynamic studies on the removal of basic dye Rhodamine-B from aqueous solution by the use of natural adsorbent perlite. Journal of Materials and Environmental Science 3, 157-170.

[68] Ayawei, N.; Ebelegi, A.N.; Wankasi, D. (2017) Modelling and interpretation of adsorption isotherms. Journal of Chemistry 2017, 3039817.

[69] Temkin, M.I.; Pyzhev, V. (1940) Kinetics of ammonia synthesis on promoted iron catalysts. Acta Physicochimica URSS 12, 327-356.

[70] Salman, M.; Rehman, R.; Farooq, U.; Tahir, A.; Mitu, L. (2020) Biosorptive Removal of Cadmium(II) and Copper(II) Using Microwave-Assisted Thiourea-Modified Sorghum bicolor Agrowaste. Journal of Chemistry 2020, 8269643.

[71] Dada, A.; Olalekan, A.; Olatunya, A.; Dada, O. (2012) Langmuir, Freundlich, Temkin and Dubinin–Radushkevich isotherms studies of equilibrium sorption of Zn2+ unto phosphoric acid modified rice husk. IOSR Journal of Applied Chemistry 3, 38-45.

[72] Ibrahim, M.; Sani, S. (2014) Comparative isotherms studies on adsorptive removal of Congo red from wastewater by watermelon rinds and neem-tree leaves. Open Journal of Physical Chemistry 4, 139-146.

[73] Shukla, S.R.; Pai, R.S.; Shendarkar, A.D. (2006) Adsorption of Ni(II), Zn(II) and Fe(II) on modified coir fibres. Separation and Purification Technology 47, 141–147.

[74] Martins, A.E.; Pereira, M.S.; Jorgetto, A.O.; Martines, M.A.; Silva, R.I.; Saeki, M.J.; Castro, G.R. (2013) The reactive surface of Castor leaf [Ricinus communis L.] powder as a green adsorbent for the removal of heavy metals from natural river water. Applied Surface Science 276, 24-30.

[75] McLintock, I. (1967) The Elovich equation in chemisorption kinetics. Nature 216, 1204-1205.

[76] Ho, Y.-S.; McKay, G. (1999) Pseudo-second order model for sorption processes. Process Biochemistry 34, 451-465.

[77] Qiu, H.; Lv, L.; Pan, B.-C.; Zhang, Q.-J.; Zhang, W.-m.; Zhang, Q.-X. (2009) Critical review in adsorption kinetic models. Journal of Zhejiang University-Science A 10, 716-724.

[78] Lagergren, S.K. (1898) About the theory of so-called adsorption of soluble substances. Svenska Vetenskapsakademiens Handlingar 24, 1-39.

[79] Ho, Y.S.; McKay, G. (2000) The kinetics of sorption of divalent metal ions onto sphagnum moss peat. Water Research 34, 735-742.

[80] Cheung, C.W.; Porter, J.F.; McKay, G. (2000) Elovich equation and modified second-order equation for sorption of cadmium ions onto bone char. Journal of Chemical Technology and Biotechnology 75, 963-970.

[81] Ho, Y.S.; McKay, G. (1998) A comparison of chemisorption kinetic models applied to pollutant removal on various sorbents. Process Safety and Environmental Protection 76, 332-340.

[82] Tseng, R.-L.; Wu, F.-C.; Juang, R.-S. (2003) Liquid-phase adsorption of dyes and phenols using pinewood-based activated carbons. Carbon 41, 487-495.

[83] Priyantha, N.; Bandaranayaka, A. (2011) Investigation of kinetics of Cr (VI)–fired brick clay interaction. Journal of Hazardous Materials 188, 193-197.

[84] Weber Jr, W.J.; Morris, J.C. (1963) Kinetics of adsorption on carbon from solution. Journal of the Sanitary Engineering Division 89, 31-59.

[85] Kannan, N.; Sundaram, M.M. (2001) Kinetics and mechanism of removal of methylene blue by adsorption on various carbons—a comparative study. Dyes and Pigments 51, 25-40.

[86] Sujana, M.; Mohanty, S. (2010) Characterization and fluoride uptake studies of nano-scale iron oxide-hydroxide synthesized by microemulsion method. International Journal of Engineering, Science and Technology 2(8), 1-12.

[87] Lima, E.C.; Hosseini-Bandegharaei, A.; Moreno-Piraján, J.C.; Anastopoulos, I. (2019) A critical review of the estimation of the thermodynamic parameters on adsorption equilibria. Wrong use of equilibrium constant in the Van't Hoff equation for calculation of thermodynamic parameters of adsorption. Journal of Molecular Liquids 273, 425-434.

[88] Govindasmay V; Sahadevan R; Subramanian S; Mahendradas D.K. (2009) Removal of malachite green from aqueous solution by perlite. International Journal of Chemical Reactor Engineering 7, 43–49.

[89] Seki Y.; Yurdako K. (2006) Adsorption of Promethazine hydrochloride with KSF montmorillonite. Adsorption 12, 89–100.

[90] Tunali S.; Özcan A.S.; Özcan A.; Gedikbey T. (2006) Kinetics and equilibrium studies for the adsorption of Acid Red 57 from aqueous solutions onto calcined-alunite. Journal of Hazardous Materials 135, 141–148.